Crystalline Silica Mediated Inflammation: Role of Mast Cells

Emma Adkins[1], Bindu Hedge[1,2], Haribabu Bodduluri[1,2]

[1]James Graham Brown Cancer Center, [2]Department of Microbiology and Immunology, University of Louisville Health Sciences Center, Louisville, KY- 40202,

Abstract

Prolonged exposure to crystalline silica (CS) leads to silicosis due to chronic inflammation and fibrosis of the lungs. Individuals with silicosis are twice as likely to develop lung cancer. A key aspect of this CS-induced inflammation is the migration of neutrophils to the lungs. The process of neutrophil recruitment to the lungs begins with the chemoattractant Leukotriene B_4 (LTB_4) binding to BLT1 and BLT2 receptors. The main producers of LTB_4 are macrophages and mast cells. Once this process has begun other mediators such as IL1-β and neutrophil active chemokines also play a role promoting the inflammation. When inhaled CS travels to the alveoli of the lungs where it enters mast cells, macrophages, and epithelial cells through phagocytosis. As the phagosome progresses, lipid bodies begin to appear in the cytosol. After fusion of the lysosome and phagosome the inflammasome protein complex appears and produces IL1-β. By inhibiting the formation of the phagolysosome, IL1-β production is stunted while LTB_4 production is heightened. This shows that the production of LTB_4 and IL1-β are triggered independently of one another. The pathway through which inflammasomes are constructed and produce IL1-β is understood, while the pathway through which LTB_4 is produced is not yet clear. The first objective of this study is to stain different cellular compartments using microscopy to determine the connection between phagocytosis and LTB_4 production in macrophages. While mast cells are known to play an important role in inflammation and produce even more LTB_4 than macrophages, little is known about the process through which this occurs. Rat basophilic leukemia (RBL) cells share many properties with mast cells. The second objective of this study is to determine if RBL cells make LTB_4 in response to CS.

Background

In 2015, lung cancer was responsible for approximately 27% of all cancer deaths, making it the number one cancer killer of both men and women (1). Factors such as smoking, genetic susceptibility and various environmental hazards are known to increase the risk of lung cancer. One of these environmental hazards is crystalline silica, the second most abundant element on the earth. Millions of workers in the US alone are exposed to CS every year. When in crystalline form silica is inhaled into the lungs where the particles become trapped and damage lung tissue. The damaged tissue eventually becomes scar tissue that forms granulomas. The damage done by CS causes the incurable, but preventable, lung disease silicosis. Individuals with silicosis are at an increased risk of developing lung cancer, making CS a human carcinogen.

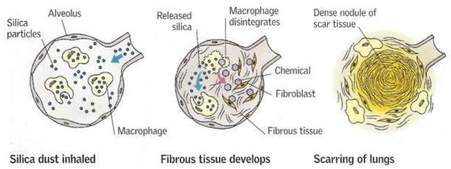

Results

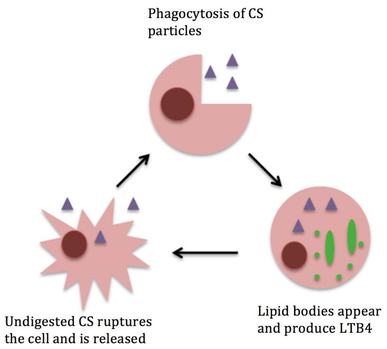

This cycle attracts neutrophils and causes chronic inflammation

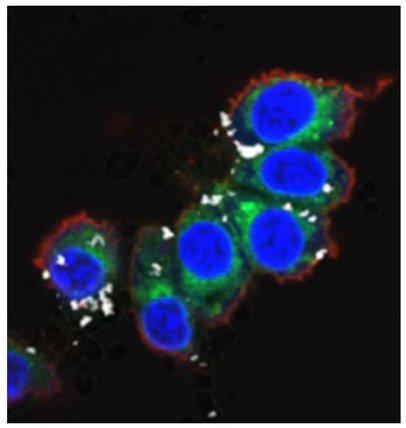

Confocal microscopy of nucleus (blue), CS (white), lipid bodies (green), and membrane (red) in a macrophage

LTB_4 Production by RBLs in Response to CS

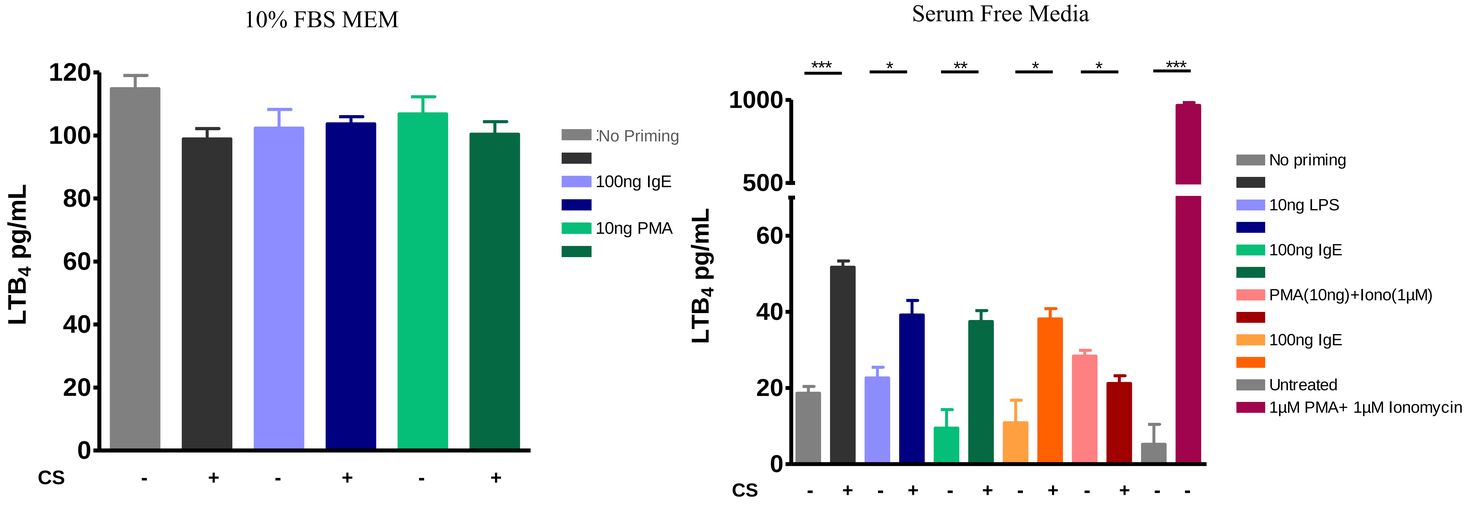

Methods

RBL-2H3 cells were plated in a 24-well cell culture plate with a cell density of $1x10^5$ cells/well. Cells adhered to the cell plate overnight in 500 μl of 10% FBS MEM. A variety of priming agents were used. Cells were primed overnight with 10 μg PMA, 100 μg IgE, 10 μg LPS, 10ng PMA+ + 1 μM Ionomycin. Before CS stimulation the cells were switched to either 200 μl of 1% FBS media or serum free media. 1 μM PMA + 1 μM Ionomycin was used as a positive control. After the cells were stimulated with 100-$\mu g/$ cm^{-2} of CS for 5 hours, the supernatant was removed and a LTB_4 Elisa was run following the manufacturers protocol to determine the levels of LTB_4 produced. Experiments were done in triplicate cultures.

Conclusions

- In 10% FBS MEM, with and without priming, CS does not induce LTB_4 production in RBL cells.
- In serum free media, with and without priming, CS induces LTB_4 production in RBL cells for all conditions except PMA (10ng)+Iono (1μM).
- CS induces the most LTB_4 production in RBL cells without priming in serum free media. This was expected because CS also induces the most LTB_4 production in bone marrow derived mast cells without priming in serum free media.
- Using RBL cells in place of mast cells will allow for studies to be completed using a more durable and accessible cell line.

Future Directions

- Refine the conditions in which CS induces LTB_4 production in RBL cells.
- Use RBL cells without priming in serum free media to study LTB_4 production in mast cells.
- Continue with confocal microscopy to determine the connection between phagocytosis and LTB_4 production.

Acknowledgements

This research was supported by National Caner Institute grant R25-CA134283 and Kentucky Lung Cancer Research Program.

References

1. Lung Cancer Fact Sheet. *Lung Health & Diseases.*
2. Crystalline Silica Exposure Health Hazard Information. *OSHA Fact Sheet.*
3. Satpathy, Shuchismita R. et al. "Crystalline Silica-Induced leukotriene B4-Dependent Inflammation Promotes Lung Tumor Growth." *Nature Communications* 6 (2015): 7064. *PMC.* Web. June 2016

Contact Information:
Emma Adkins emma.adkins@uky.edu | Haribabu Bodduluri H0bodd01@louisville.edu

Nutritive Intake Relates to Activated Cytotoxic T Cells in Lung Cancer Patients

Kait Adkisson[1], Christina Albert, BA[1], Sandra Sephton, PhD[2,3], Elizabeth Cash, PhD[1,2,3]

[1]Department of Otolaryngology-HNS & Communicative Disorders
[2]Department of Psychological & Brain Sciences
[3]James Graham Brown Cancer Center

Abstract

Knowledge of chemo-preventative nutrition far outweighs our familiarity with post-diagnosis nutrition and the implication of nutritional intake on factors that may influence lung cancer progression. We predicted percent energy from fat would increase triglyceride (TG) and LDL levels as well as dysregulate immune response upregulating natural killer (NK) cells, cytotoxic T-lymphocyte counts (CTL), and stimulated of TNF-α and IL-6. Additionally we postulated that an increase in fruit and vegetable servings would decrease serum TG and LDL levels while decreasing activation of these inflammatory and immune responses.

Lung cancer patients (n = 62, 34 female) were recruited from the Brown Cancer Center. Patients were within 5 years of diagnosis and had primarily non-small-cell lung cancer, with disease stage ranging from early to advanced. Self-report questionnaires assessing fruit and vegetable intake and percent energy from fat were collected. Lipid panels provided TG and LDL levels. Flow cytometry characterized serum NK (CD69) and CTL (CD11b) cell activation counts. PHA stimulated serum TNF-α and IL-6 levels. Preliminary bivariate Spearman correlations were used to determine potential control variables by assessing relationships between demographic, clinical, social, and medical variables with outcome variables. Hierarchical linear regressions adjusted for age at diagnosis and cancer stage. Nutrition indicators were entered as independent variables with lipid indicators and factors of activated immunity as dependent variables.

Nutritional intake was not significantly related to lipid indicators. Greater fruit and vegetable intake were associated with a lower activated CTL count (partial r= -.322, p=.027). Nutritional intake did not relate to NK cell counts or PHA stimulated immune markers.

Nutritive intake of fruit, vegetable and fat has no significant relationship to lipid counts. CTL remains independent of percent energy from fat while an increase in fruit and vegetable serving lowers activated CTL count. A diet consisting of greater fruit and vegetable intake will decrease the functionality of CTL response in lung cancer patients which could be disadvantageous to survival and tumor clearance. Inflammatory response and lipid indicators appear uninfluenced by nutrition intake.

Funding support provided by R25-CA134283 grant from the National Cancer Institute

Introduction

Lung cancer is the most deadly malignant disease with an austere 15% five year survival rate (1). Contributors to prognosis include inflammation and the cachexia, anorexia and overall poor nutrition which accompanies approximately 60% of these cases (2). The impact of a healthy diet on immune function is well-understood. However, the impact of a cancerous mediator on these functions remains unclear. Equipping ourselves with nutritional strategies to intervene and looking at nutrition as a way to support treatment in a challenging disease process could potentially be life saving for these patients. Research lends support to this idea: Subjective Global Assessment scores in lung patients are significantly higher than in patients with benign cancers (p=.005; 4) posing the question of nutrition's role in poor prognosis.

Nutritive intake of fats, fruits and vegetables, have demonstrated relationships to immune function (3). Presence of immune markers like CTL and NK cells are characterized by their roles in tumor degradation and hold prospective influence by nutritional intake due to their nature (5). Inflammatory markers such as TNF-α and IL-6 are known to negatively relate to nutritional status, and are upregulated in lung cancer (6).

Hypotheses

- Percent energy from fat will relate to increased triglyceride (TG) and LDL levels as well as dysregulated immune responses (increased NK and CTL counts, and increases to stimulated TNF-α and IL-6 levels).
- Increased fruit and vegetable servings will relate to decreased serum TG and LDL levels, and decreased activation of these inflammatory and immune responses.

Methods

Lung cancer patients (n = 62, 34 female) were recruited from the Brown Cancer Center. Patients were within 5 years of diagnosis and had primarily non-small-cell lung cancer, with disease stage ranging from early to advanced. Self-report questionnaires assessing fruit and vegetable intake and percent energy from fat were collected and blood samples were drawn. Lipid panels provided triglyceride (TG) and LDL levels. Whole blood samples were subjected to flow cytometry for measurement of CD3/CD8 Cytotoxic T-lymphocyte (CTL, (CD11b)) count and CD3-/CD56 natural killer (NK, (CD69)) cell count. PHA stimulated peripheral blood mononuclear cells were assayed to quantify TNF-α and IL-6 levels. Preliminary bivariate Spearman correlations were used to determine potential control variables by assessing relationships between demographic, clinical, social, and medical variables with outcome variables. Hierarchical linear regressions adjusted for age at diagnosis and cancer stage. Nutrition indicators were entered as independent variables with lipid indicators and factors of activated immunity as dependent variables.

Results

Preliminary bivariate Spearman correlations were used to determine potential control variables by assessing relationships between cytokines of interest and demographic, clinical, social, and medical variables. All were non-significant. Emperical control variables of age at diagnosis, and stage of disease, were entered in all tests of hypotheses.

Table 1: Demographic and clinical characteristics

	Mean	SD	N	%
Age	61.03	8.99		
Gender				
Male			27	43.5
Female			35	56.5
Race				
Black			7	11.3
Hispanic			1	1.6
White			53	85.5
Other			1	1.6
Income				
<20K			19	30.6
20-39K			23	37.1
>40K			20	32.3
Pack-Years	58.75	39.51		
Current Smoker			22	39.3
Stage				
I			27	44
II			7	11
III			17	27
IV			7	11
Small Cell				
Limited			2	3
Extensive			2	3

Table 2: Study Variables

	N	Mean	SD	Min	Max
Mean daily fruit/vegetable servings	62	4.58	2.22	0	8.44
Mean daily % energy from fat	62	33.15	2.53	28.26	40.96
Triglycerides	54	198.22	126.15	49.00	733.00
LDL	51	104.98	32.35	47.00	184.00
Activated CTL (CD11b) count	52	305.72	204.09	39.00	887.92
Activated NK (CD69) count	51	26.68	30.88	0.09	183.03
PHA-stimulated TNF-α, pg/mL	52	5.99	6.68	1.50	29.23
PHA-stimulated IL-6, pg/mL	52	56.52	87.73	1.50	416.09

Hierarchical linear regression adjusted for age at diagnosis and tumor stage entered fruit and vegetable intake as the independent variable, with activated cytotoxic T lymphocyte (CTL) count, activated NK cell count, PHA-stimulated TNF-a and IL-6 as the dependent variables in separate models. Results suggested that higher fruit and vegetable intake was associated with significantly lower CTL count (Δr^2=.087, partial r=-.322., p=.027).All other analyses were non-significant.

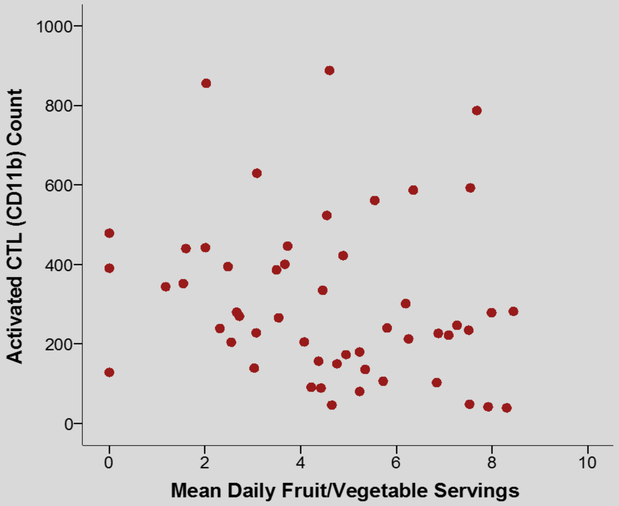

Figure 1. Nutritive intake of fruits and vegetables were significantly associated with decreased activated CTL count.

Conclusions

- There is reason to further investigate nutrition as a mediator of immune and inflammatory response due to the association of fruit and vegetable intake and CTL count.
- A diet consisting of greater fruit and vegetable intake may decrease the functionality of CTL response in lung cancer patients which could be disadvantageous to survival and tumor clearance.
- Nutritive intake of fruit, vegetable and fat had no significant relationship to lipid counts. Our results were inconclusive regarding TNF-α, and no significant relationship was found between nutrition and IL6.
- Possible additional mediators not identified through this study may contribute as factors of causation for dysregulated immune responses.
- Use of a larger sample size and a more detailed nutrition questionnaire outlining the specificity of intake would lend greater understanding of the role nutrition takes in lung cancer.

References

1. Bremnes, R. M., Busund, L. T., Kilvær, T. L., Andersen, S., Richardsen, E., Paulsen, E. E., ... & Dønnem, T. (2016). The Role of Tumor-Infiltrating Lymphocytes in Development, Progression, and Prognosis of Non–Small Cell Lung Cancer. Journal of Thoracic Oncology, 11(6), 789-800.
2. Utech, A. E., Tadros, E. M., Hayes, T. G., & Garcia, J. M. (2012). Predicting survival in cancer patients: the role of cachexia and hormonal, nutritional and inflammatory markers. Journal of cachexia, sarcopenia and muscle, 3(4), 245-251.
3. Steinmetz, K. A., & Potter, J. D. (1991). Vegetables, fruit, and cancer. II. Mechanisms. Cancer Causes & Control, 2(6), 427-442.
4. Kovarik, Miroslav, Miloslav Hronek, and Zdenek Zadak. "Clinically relevant determinants of body composition, function and nutritional status as mortality predictors in lung cancer patients." Lung Cancer 84.1 (2014): 1-6.
5. Maher, J., & Davies, E. T. (2004). Targeting cytotoxic T lymphocytes for cancer immunotherapy. British journal of cancer, 91(5), 817-821.
6. Gullett, N. P., Mazurak, V., Hebbar, G., & Ziegler, T. R. (2011). Nutritional interventions for cancer-induced cachexia. Current problems in cancer, 35(2), 58.

Acknowledgements

Research supported by a grant (R25-CA134283) from National Cancer Institute and the School of Medicine Summer Research Scholar Program.

The effect of reactivation of pRb on the metabolism of cancer cells

Yomna Amer[1], Traci Kruer[2], Brian Clem[1,2].
Departments of Biochemistry and Molecular Genetics, University of Louisville, James Graham Brown Cancer Center, NCI R25 Cancer Education Program

Background

The retinoblastoma protein, Rb, is a tumor suppressor that is commonly found to be inactivated in cancer cells. The anti-proliferative activity of RB is mediated by its ability to inhibit the transcription of genes that are required for cell-cycle progression, like Cyclin A, which is targeted and repressed by active pRb.[1] Phosphorylation of pRb allows E2F-DP transcription factors to dissociate from pRb and become active. When E2F is free it activates target genes like cyclin A, which pushes the cell through the cell cycle.[2] Expression of constitutively active PSM-RB, which is a truncated/mutated form of pRb that cannot be phosphorylated, results in decreased cell number and division.

Objective

The aim of our study is to test how the reactivation of the Rb protein will affect the metabolism of non-small cell lung cancer cells. We inserted a constitutively active form of Rb (PSM-Rb) into NSCLC cells and measured the metabolism in cancer cells compared to the empty plasmid PCDNA3. The metabolism was measured through glucose uptake and glycolysis. Our study's aim was to whether activation of the Rb protein disrupts the metabolism of A549 NSCLC cells.

Methods

We cloned PSM-Rb into PCDNA3 mammalian expression vector and ran western blots to ensure the expression of PSM-Rb. PSM and the empty plasmid, PCDNA3 were transfected into A549 NSCLC for 24 or 48 hours. We measured the effect of changing the concentrations of transfected plasmid, 1 µg or 2 µg on the cell count, and measured the metabolism of PSM vs. PCDNA3 cells. To measure glucose uptake, C14 radioactive 2-deoxy-glucose was added to the cells in glucose-free media. Cells were incubated for one hour, washed 3X with ice cold RPMI glucose-free media, and lysed using 0.1% SDS. The lysates were then collected, and scintillation fluid was added to measure the radioactive activity of C14 within the cells. To measure glycolysis, media was changed to 500 µl of regular media in each well and 2 µl of 3H-glucose were added to each well and incubated for an hour. The media was collected and spun at 8000 rpm in the centrifuge to pellet any cells that may be in the media. 150 µl of the media was added to a 500 µl tube within a scintillation vial containing 1ml of H_2O. The vials were incubated for 48 hours to allow the for the evaporation of $3H_2O$ into the surrounding H_2O, and then 5mls of scintillation fluid were added and radioactivity was measured. The radioactivity indicates the amount of $3H_2O$ produced by enolase, an enzyme within glycolysis. The cells in the well are lysed with 0.1% SDS for 5 minutes, and were collected to measure the protein concentration.

Results

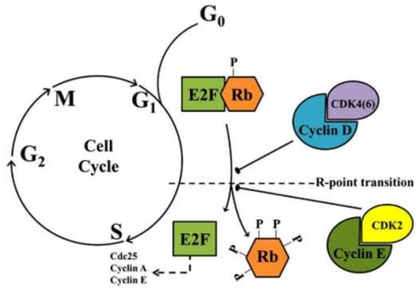

Figure 1. Hyper-phosphorylation of pRb allows E2F transcription factors to dissociate from pRb and become active, and hence allows cell-cycle progression.

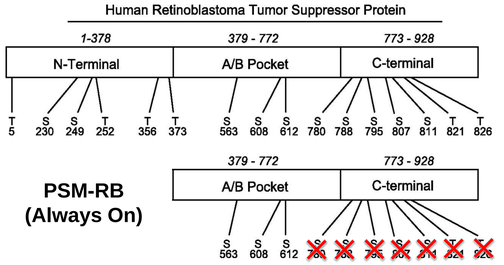

Figure 2. Comparison of WT Rb to the constitutively active PSM-Rb. PSM-Rb lacks the N-terminal domain and contains phosphorylation site mutations (alanine) within the C-terminus, which allows for PSM-Rb to be always on.

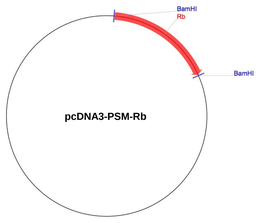

Figure 3. Cloning of PSM into the PCDNA3 mammalian expression vector was done at the BamH1 restriction site.

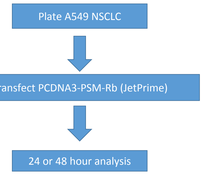

Figure 4. Flowchart.

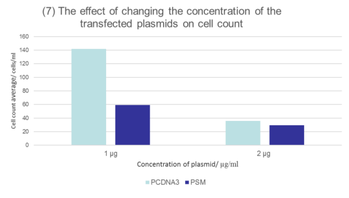

Figure 5. The cloning of PSM was successful since the western blots showed Rb specific protein bands that were present in PSM-Rb.

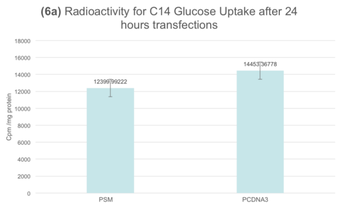

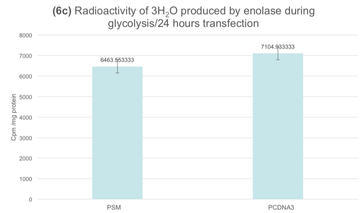

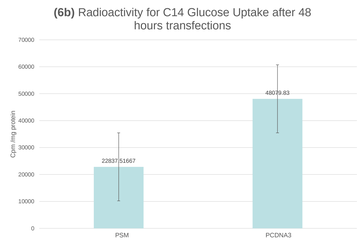

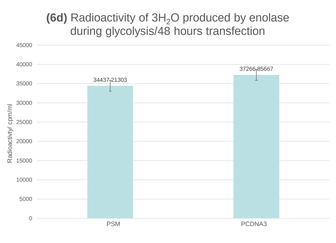

Figure 6. The graphs show the radioactivity in (a), (b) ^{14}C glucose uptake, and (c), (d) ^{3}H H_2O release of PSM and PCDNA3 after 24 or 48 hour transfections. The 48-hour transfections are needed for PSM-Rb to be effective and to show some difference compared to PCDNA3 with regards to ^{14}C glucose uptake. The ^{3}H H_2O release results were not significantly different for PSM and PCDNA3 at neither 24 nor 48-hour transfections. **Figure 7.** Increasing the concentration of the transfected plasmids at 72 hours decreased the number of cells per ml in both PSM and PCDNA3. PSM showed a lower number of cells than PCDNA3 at both 1 µg and 2 µg plasmid concentrations.

The cloning of PSM was successful since the results of the western blots showed Rb specific protein bands that were present in PSM-Rb, but were absent on PCDNA3 samples. Cell counts of PSM and PCDNA3 showed significant decrease in cell numbers for PSM compared to that of PCDNA3. Increasing the transfected plasmid concentration from 1 µg to 2 µg decreased the cell count for both PSM and PCDNA3. Our results for 24 hour transfections show no significant difference between PSM and PCDNA3 on glucose uptake nor in glucose flux (glycolysis). However, 48 hour transfections show substantial decreases between PSM and PCDNA3 for the glucose uptake and the glycolysis measurements.

Conclusions

The lower cell count for PSM compared to PCNDA3 confirms the active effect pRb has on attenuating the cell-cycle progression and division which is evidence for its role as a tumor suppressor in cancer cells. Our experiments also suggest that 24-hour transfections were not effective in showing a significant difference between the metabolism of PSM and the PCDNA3 control. However, the 48-hour transfection showed significant results for the glucose uptake in PSM vs PCDNA3 cells. Hence, the cells need 48 hours for the Rb protein from the PSM plasmid to be effective. Our data also suggest that the metabolism is lower in cells that express the active Rb protein. Our conclusion is that the activation of the Rb protein disrupts the growth and glucose metabolism of non-small cancer cells in the A549 cell line.

Acknowledgments

NCI R25 grant support University of Louisville Cancer Education Program NIH/NCI (R25- CA134283)
Brown Graham Cancer Center, University of Louisville, Clem lab: Romaysa Biyik, Lindsey Reynolds, Stephanie Metcalf, and Miriam Reynolds

References

1) Knudsen KE[1], Fribourg AF, Strobeck MW, Blanchard JM, Knudsen ES. (09/24/1999). Cyclin A is a functional target of retinoblastoma tumor suppressor protein-mediated cell cycle arrest. *PubMed.gov*, 274(39):27632-41 Retrieved from http://www.ncbi.nlm.nih.gov/pubmed/10488103
2) Pietro Garofalo. (25/03/2010). G1/S Checkpoint. *flipper e nuvola. Retrieved from:* http://flipper.diff.org/app/pathways/info/2699

UofL Design and Print

Sensitizing Pancreatic Cancer Cells to Chemotherapeutics by Modulating Intracellular Iron Homeostasis

Kyle D. Bilyeu, Lilibeth Lanceta, John Eaton, Ph.D., Chi Li, Ph.D.
Molecular Targets Group, James Graham Brown Cancer Center, Department of Pharmacology and Toxicology, University of Louisville, Louisville, KY 40202

Abstract

Currently, the only successful treatment for pancreatic cancer is invasive surgery. Previous studies to develop chemotherapeutic agents targeting pancreatic tumors have not led to any identifiable success. Due to the extreme vascularization of pancreatic tumors, we hypothesized that the overexpression of heme oxygenase-1 (HO-1) is responsible for the resistance of pancreatic cancer cells to chemotherapeutic drugs. Coinciding with elevated HO-1expression, pancreatic cancer cells have increased expression of the heavy chain subunit of the intracellular iron-storage protein ferritin (FTH-1). To test our hypothesis, a series of experiments were designed to modulate the expression levels of HO-1 and FTH-1 in the human pancreatic cancer cell line Mia Paca-2, to test effects on the cytotoxicity of the platinum-based chemotherapeutic agent oxaliplatin. Reducing HO-1 expression by small interfering RNA (siRNA) sensitized Mia Paca-2 cells to oxaliplatin. Similarly, oxaliplatin induced more cell death in cancer cells with transiently and stably decreased FTH-1 expression. Furthermore, inhibiting HO-1 enzymatic activities by zinc protoporphyrin-9 promoted cytotoxic activities of oxaliplatin. Our studies provide evidence that intracellular iron homeostasis is involved in the pancreatic tumor cells' responses to oxaliplatin. We are currently exploring the molecular mechanism of how modulating intracellular iron homeostasis sensitizes pancreatic tumor cells to chemotherapeutics. We expect these approaches will lead to a usable, therapeutic treatment for pancreatic cancer.

Objectives

- Study whether reducing the expression of HO-1 in pancreatic tumor cells improves the therapeutic effects of oxaliplatin.
- Investigate whether expression levels of FTH-1 are involved in the pancreatic tumor cells' responses to oxaliplatin.
- Examine whether inhibiting HO-1 enzymatic activities by zinc protoporphyrin-9 sensitizes pancreatic cancer cells to oxaliplatin.

Results

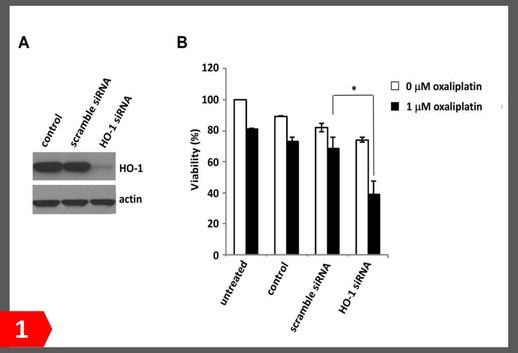

1

Figure 1

A) Mia Paca-2 cells were cultured in 6-well plates (9 x10^4/well) for 24 hours. Cells were transfected with 40 nM scramble siRNA or 40 nM HO-1 siRNA. 24 hours later cell lysates were collected and 20 μg of protein samples were loaded on a gel. The blot was probed with anti-HO-1 or anti-actin antibodies.
B) Mia Paca-2 cells were seeded in 12-well plates (4x10^4/well) for 24 hours. Cells were untransfected or transfected with 40 nM scramble siRNA or 40 nM HO-1 siRNA. Following 24 hour-treatment with DMSO or 1 μM oxaliplatin, cell viability was measured using Alamar Blue reduction at 37ºC for two hours. Mean ± S.D., n=3. P < 0.05 (*) Student's unpaired t test.

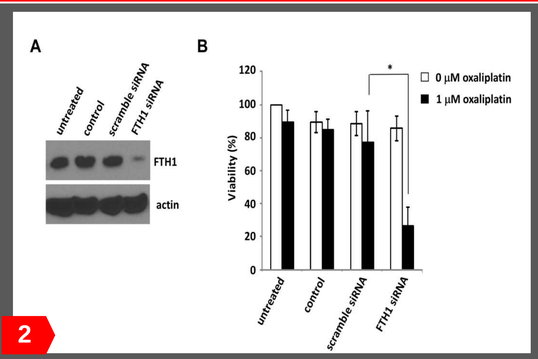

2

Figure 2

A) Mia Paca-2 cells were seeded in 6-well plates (9 x10^4/well) for 24 hours. Cells were transfected with 40 nM scramble siRNA or 40 nM FTH-1 siRNA for 24 hours. Whole cell lysates were acquired. Expression of FTH-1 and actin was determined by western blot.

B) Following 24 hour-incubation in 12-well plates (4 x10^4/well), Mia Paca-2 cells were untransfected or transfected with 40 nM scramble siRNA or 40 nM FTH-1 siRNA for 24 hours. Cells were then treated with DMSO or 1 μM oxaliplatin. Cell viability was measured using Alamar Blue reduction at 37ºC. Mean ± S.D., n=3. P < 0.05 (*) Student's unpaired t test.

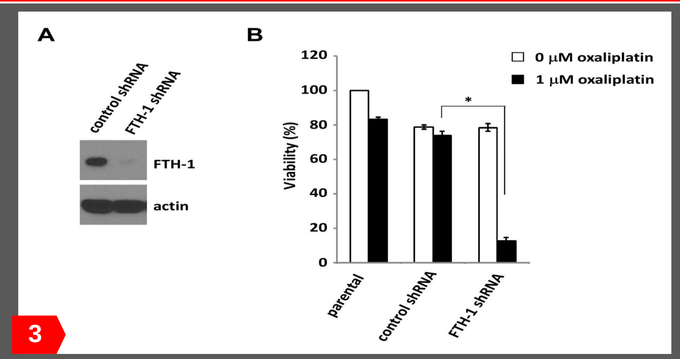

3

Figure 3

A) FTH-1 expression in Mia Paca-2 cells was stably reduced by lentiviral infection. Cells were cultured with the medium from transfected 293T cells containing lentivirus. Cells with stably reduced FTH-1 expression were acquired by culturing in the presence of 5 μg/ml puromycin. Expression of FTH-1 was determined by western blot.

B) The indicated Mia Paca-2 cells were treated with DMSO or 1 μM oxaliplatin for 24 hours. Cell viability was measured using Alamar Blue reduction at 37ºC for two hours. Data are presented as Mean ± S.D. of 3 independent experiments. P < 0.05 (*) Student's unpaired t test.

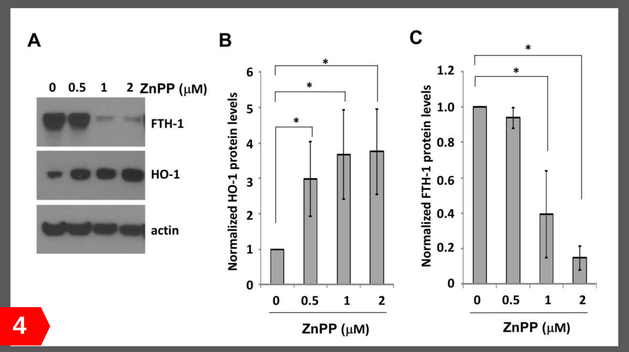

4

Figure 4

A) Mia Paca-2 cells were cultured in 6-well plates (9 x10^4/well) for 24 hours. Cells were treated with 0, 0.5, 1, or 2 μM Zinc Protoporphyrin-IX (ZnPP) for 24 hours. Whole cell lysates were acquired. Expression of HO-I, FTH-1 and actin was determined by western blot.
B) The intensities of HO-1 and actin shown in (A) were quantified using ImageJ software (NIH). The relative HO-1 expression was normalized to the corresponding actin levels. Mean ± S.D., n=3. P < 0.05 (*) Student's unpaired t test.
C) Normalized FTH-1 in ZnPP-treated cells as in (A). The relative FTH-1 levels were normalized with the values of corresponding actin levels. Mean ± S.D., n=3. P < 0.05 (*) Student's unpaired t test.

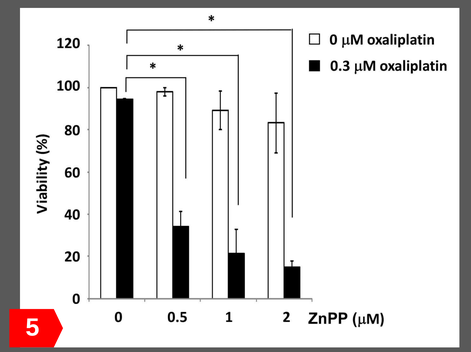

5

Figure 5

Mia Paca-2 Cells were cultured in 12-well plates (4.0x10^4/well) for 24 hours. The cells were treated with 0, 0.5 μM, 1 μM, or 2 μM ZnPP for 24 hours. Following ZnPP incubation, the cells were treated with DMSO or 0.3 μM oxaliplatin and incubated for 24 hours. After incubation, viability was assessed by Alamar Blue reduction during 2 hour-incubation at 37ºC. Data are shown as Mean ± S.D. of 3 independent experiments. P < 0.05 (*) Student's unpaired t test.

Conclusions

- Decreasing HO-1 expression in pancreatic tumor cells sensitizes pancreatic cancer cells to oxaliplatin.
- Reducing the expression of FTH-1 transiently and stably enhances cytotoxic activities of oxaliplatin in pancreatic tumor cells.
- The HO-1 enzymatic activity inhibitor zinc protoporphyrin-9 promotes therapeutic effects of oxaliplatin.

Acknowledgments

Funding for this project was provided by R25-CA134283 grant from National Cancer Institute. This research was also supported by a Undergraduate Research Grant from Executive Vice President For Research and Innovation Internal Grant Program at University of Louisville.

Impact of High Order Interactions between Inflammatory and Immune Response Genes in Prostate Cancer among men of African Descent

Christian Bradley, Tiana Martin, Dominique Reed, LaCreis R. Kidd
Department of Pharmacology and Toxicology and James Graham Brown Cancer Center

INTRODUCTION

- Prostate cancer (PCa) afflicts over one million men each year worldwide.
- There is a 28% 5-year survival rate for metastatic PCa.
- PCa risk factors include age, lifestyle, environmental factors, race, and chronic/recurrent inflammation.
- African-American men have higher incidence and mortality rates compared to any other races.
- The role of toll-like receptors (TLRs) in the innate inflammatory response is to induce the expression of immune response and pro-inflammatory cytokines, chemokines, and interleukins.
- Dysregulation of TLR signaling pathways is proposed to lead inflammatory induced cancers, including PCa.
- Our lab has revealed significant interactions among *TLR6* rs2381289, *TLR10* rs11096957, and *IRF3* rs2304206 as the best 3-factor predictor of PCa risk among U.S. and Jamaican men.

Figure 1. TLR SIGNALING PATHWAY

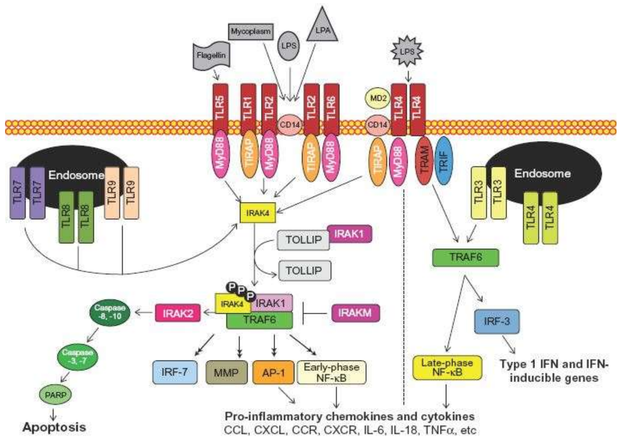

RESEARCH GAP

The impact of two or more sequence variants in TLR, cytokine, and chemokine associated genes jointly modifying PCa risk among men of African descent remains understudied.

RESEARCH OBJECTIVE

Evaluate the individual and joint modifying effects of inflammatory and immune response associated sequence variants in relation to PCa risk among men of African descent.

HYPOTHESIS

Inheritance of one or more sequence variants (linked with cell survival, pro-inflammatory response, immune/tumor cell migration, chemotaxis, invasion, angiogenesis, and lymph node metastasis) will have increased PCa risk relative to men who inherit the wildtype genotype.

STUDY DESIGN

814 men were recruited from cancer screening programs, hospitals, or cancer centers located in Washington, D.C., South Carolina, and Kingston, Jamaica.

- Total population: 603 U.S. men and 211 Jamaican men
  - U.S. population: 170 cases, 433 controls
  - Jamaican population: 109 cases, 102 controls

METHODS

To test the hypothesis, we evaluated individual and joint modifying effects of toll-like (n = 33), cytokine (n = 36), and chemokine (n = 51) associated sequence variants among men of African descent.

All analyses were performed using statistical analysis software (SAS 9.4) and entropy-based multi-dimensionality reduction 2.0 beta 8.4

CLINICAL RELEVANCE

The discovery of significant interactions between inflammatory and immune response associated SNPs in relation to PCa risk may help:

- improve PCa detection strategies;
- discern between lethal and non-lethal disease based on one's genetic composition; and
- identify new immune/inflammatory response related gene targets needed for the effective treatment of aggressive prostate cancer.

RESULTS

Table 1. Role of TLR Sequence Variants on PCa risk among men of African descent.

Genes dbSNP ID Position Function	Genotype	Controls n (%)	Cases (%)	Age Adjusted OR (95% CI)	P-value	P-trend
TLR6	GG	302 (37.24)	140 (17.26)	1.00 (referent)		0.198
rs2381289	GA	201 (24.78)	124 (15.29)	1.45 (1.01, 2.08)	0.043	
	AA	30 (3.70)	14 (1.73)	1.20 (0.53, 2.74)	0.662	
	AA vs (GG+GA)			1.02 (0.46, 2.29)	0.956	
	(AA+GA)	231 (28.48)	138 (17.02)	1.43 (1.01, 2.03)	0.046	
TOLLIP	AA	187 (23.14)	85 (10.52)	1.00 (referent)		0.686
rs5743899	GA	235 (29.08)	140 (17.33)	1.54 (1.04, 2.30)	0.032	
	GG	110 (13.61)	51 (6.31)	0.26 (0.76, 2.07)	0.369	
	GG vs (AA+AG)			0.99 (0.64, 1.53)	0.948	
	(GG+AG)	345 (42.70)	191 (23.64)	1.50 (1.03, 2.18)	0.035	
TOLLIP	GG	189 (23.25)	104 (12.79)	1.00 (referent)		0.26
rs3168046	GA	239 (29.40)	131 (16.11)	0.85 (0.58, 1.25)	0.419	
miRNA	AA	106 (13.04)	44 (5.41)	0.59 (0.35, 0.98)	0.043	
	AA vs (GG+GA)			0.64 (0.40, 1.02)	0.063	
	(AA+GA)	345 (42.44)	175 (21.53)	0.77 (0.54, 1.10)	0.155	
IRF3	GG	457 (56.21)	245 (30.14)	1.00 (referent)		0.178
rs968457	GA	70 (8.61)	32 (3.94)	0.76 (0.44, 1.31)	0.328	
Splicing (ESE or ESS)	AA	8 (0.98)	1 (0.12)	0.07 (0.01, 0.75)	0.028	
nsSNP	AA vs (GG+GA)			0.07 (0.01, 0.77)	0.029	
benign	(AA+GA)	78 (9.59)	33 (4.06)	0.67 (0.39, 1.14)	0.137	
TLR1	GG	164 (20.17)	99 (12.18)	1.00 (referent)		0.363
rs5743604	GA	260 (31.98)	121 (14.88)	0.64 (0.43, 0.95)	0.026	
	AA	111 (13.65)	58 (7.13)	0.90 (0.55, 1.46)	0.66	
	AA vs (GG+GA)			1.17 (0.76, 1.79)	0.483	
	(AA+GA)	371 (45.63)	179 (22.02)	0.71 (0.49, 1.03)	0.072	

Table 2. Validation of a Cytokine -TLR Complex Interaction along IRAK4-TOLLIP Axis and PCa among Men of African Descent using MDR.

Best Model (dbSNPID#)	Interactions	Cross Validation Consistency (CVC)	Average Testing Accuracy (ATA)	Permutation Testing p-value
One Factor				
TNF_rs673	69	6/10	0.571	0.0735
Two Factor				
IRAK4_rs4251520				
TOLLIP_rs5743899	2346	9/10	0.606	≤0.001
Three Factor				
IRAK4_rs4251520				
TOLLIP_rs5743899				
IL1RN_rs315951	52394	9/10	0.653	≤0.001

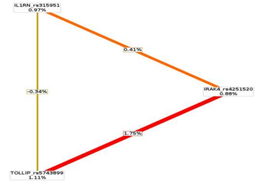

Figure 2. Synergistic 3-way Cytokine-TLR interaction along IRAK4-TOLLIP Axis identified as significant PCa predictor among Men of African Descent using entropy based analysis.

Table 3. Role of Cytokine Sequence Variants on PCa risk among men of African descent.

Genes dbSNP ID Position Function	Genotype	Controls n (%)	Cases (%)	Age Adjusted OR (95% CI)	P-value	P-trend
IL1R2	GG	211 (25.92)	87 (10.69)	1.00 (referent)		0.01
rs11886877	GA	265 (32.56)	149 (18.30)	1.34 (0.91, 1.96)	0.058	
Intron 1	AA	59 (7.25)	43 (5.28)	1.87 (1.08, 3.23)	0.016	
	AA vs (GG+GA)			1.57 (0.96, 2.58)	0.074	
	(AA+GA)	324 (39.80)	192 (23.59)	1.44 (0.99, 2.07)	0.021	
IL1A	CC	357 (43.91)	195 (23.99)	1.00 (referent)		0.104
rs17561	CA	155 (19.07)	82 (10.09)	1.01 (0.69, 1.48)	0.86	
Exon 4	AA	22 (2.71)	2 (0.25)	0.41 (0.09, 1.88)	0.016	
Splicing	AA vs (CC+CA)			0.41 (0.09, 1.87)	0.016	
benign	(AA+CA)	177 (21.77)	84 (10.33)	0.96 (0.66, 1.40)	0.378	
IL10RA	GG	268 (33.13)	134 (16.56)	1.00 (referent)		0.161
rs4252243	GA	234 (28.92)	115 (14.22)	0.82 (0.57, 1.18)	0.892	
TFBS	AA	30 (3.71)	28 (3.46)	1.57 (0.79, 3.13)	0.028	
	AA vs (GG+GA)			1.73 (0.89, 3.36)	0.021	
	(AA+GA)	264 (32.63)	143 (17.68)	0.90 (0.63, 1.28)	0.589	
IL1A	AA	358 (43.98)	196 (24.08)	1.00 (referent)		0.089
rs2856836	GA	155 (19.04)	81 (9.95)	0.99 (0.67, 1.45)	0.776	
miRNA	GG	22 (2.70)	2 (0.25)	0.40 (0.09, 1.87)	0.016	
	GG vs (AA+AG)			0.41 (0.09, 1.87)	0.016	
	(GG+AG)	177 (21.74)	83 (10.20)	0.94 (0.65, 1.37)	0.333	
IL1RN	GG	144 (17.76)	89 (10.97)	1.00 (referent)		0.061
rs315951	CG	267 (32.92)	137 (16.89)	0.83 (0.55, 1.24)	0.236	
miRNA	CC	123 (15.17)	51 (6.29)	0.58 (0.35, 0.97)	0.052	
	CC vs (GG+GC)			0.66 (0.43, 1.02)	0.129	
	(CC+GC)	390 (48.09)	188 (23.18)	0.75 (0.51, 1.10)	0.124	
TNF	GG	368 (45.26)	170 (20.91)	1.00 (referent)		0.081
rs1800629	GA	153 (18.82)	103 (12.67)	1.48 (1.02, 2.15)	0.018	
5' near gene	AA	14 (1.72)	5 (0.62)	1.34 (0.38, 4.80)	0.619	
TFBS	AA vs (GG+GA)			1.18 (0.324 4.19)	0.467	
	(AA+GA)	167 (20.54)	108 (13.28)	1.49 (1.03, 2.15)	0.029	
TNF	GG	364 (44.88)	168 (20.72)	1.00 (referent)		0.19
rs673	GA	156 (19.24)	106 (13.07)	1.47 (1.02, 2.13)	0.018	
5' near gene	AA	15 (1.85)	2 (0.25)	0.46 (0.09, 2.34)	0.097	
TFBS	AA vs (GG+GA)			0.41 (0.08, 2.06)	0.069	
	(AA+GA)	171 (21.09)	108 (13.32)	1.42 (0.99, 2.05)	0.042	

Table 4. Cytokine Complex Interaction along IL1β-IL1α-IL1RN Axis and PCa among U.S. Men Validated using MDR.

Best Model (dbSNPID#)	Interactions	Cross Validation Consistency (CVC)	Average Testing Accuracy (ATA)	Permutation Testing p-value
One Factor				
TNF_rs673	36	7/10	0.599	≤0.001
Two Factor				
IL1RN_rs315951				
TNF_rs673	630	5/10	0.632	≤0.001
Three Factor				
IL1B_rs1143627				
IL1A_rs1800587				
IL1RN_rs315951	7140	9/10	0.659	≤0.001

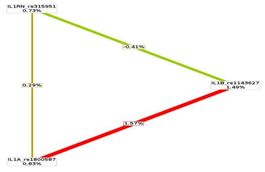

Figure 3. Synergistic 3-way Cytokine Interaction along IL1α-IL1β-IL1RN Axis identified as an effective PCa predictor among U.S. Men using entropy based analysis.

Table 5. Role of Chemokine Sequence Variants on PCa risk among men of African descent.

Genes dbSNP ID Position Function	Genotype	Controls n (%)	Cases (%)	Age Adjusted OR (95% CI)	P-value	P-trend
CCL5	GG	150 (18.45)	111 (13.65)	1.00 (referent)		0.001
rs2107538	GA	270 (33.21)	124 (15.25)	0.72 (0.49, 1.06)	0.098	
5' near gene	AA	114 (14.02)	44 (5.41)	0.53 (0.32, 0.89)	0.016	
TFBS	AA vs (GG+GA)			0.65 (0.41, 1.02)	0.063	
	(AA+GA)	384 (47.23)	168 (20.66)	0.66 (0.46, 0.96)	0.028	
CCR7	AA	151 (18.57)	55 (6.77)	1.00 (referent)		0.031
rs3136685	GA	237 (29.15)	139 (17.10)	1.87 (1.19, 2.94)	0.007	
Intron 1	GG	146 (17.96)	85 (10.46)	1.40 (0.86, 2.30)	0.179	
	GG vs (AA+AG)			0.92 (0.62, 1.35)	0.667	
	(GG+AG)	383 (47.11)	224 (27.55)	1.66 (1.09, 2.54)	0.018	
CCL5	TT	147 (18.08)	114 (14.02)	1.00 (referent)		0.002
rs3817655	AT	278 (34.19)	115 (14.15)	0.56 (0.38, 0.83)	0.004	
Intron 2	AA	110 (13.53)	49 (6.03)	0.53 (0.32, 0.87)	0.013	
TFBS	AA vs (TT+TA)			0.74 (0.47, 1.16)	0.191	
	(AA+TA)	388 (47.72)	164 (20.17)	0.56 (0.39, 0.81)	0.002	
CCR5	GG	194 (24.07)	85 (10.55)	1.00 (referent)		0.004
rs1799988	GA	227 (28.16)	107 (13.28)	0.84 (0.56, 1.26)	0.406	
UTR'5	AA	108 (13.40)	85 (10.55)	1.39 (0.89, 2.19)	0.151	
TFBS	AA vs (GG+GA)			1.52 (1.02, 2.26)	0.04	
	(AA+GA)	335 (41.56)	192 (23.82)	1.01 (0.70, 1.46)	0.951	
CCL2	AA	169 (20.79)	345 (42.44)	1.00 (referent)		0.525
rs1024611	GA	103 (12.67)	168 (20.66)	1.51 (1.04, 2.18)	0.03	
TFBS	GG	7 (0.86)	21 (2.58)	1.17 (0.40, 3.44)	0.777	
	GG vs (AA+AG)			1.01 (0.35, 2.92)	0.992	
	(GG+AG)	110 (13.53)	189 (23.25)	1.48 (1.03, 2.12)	0.035	
CXCR2	GG	230 (28.29)	434 (53.38)	1.00 (referent)		0.793
rs11574752	GA	43 (5.29)	99 (12.18)	0.88 (0.55, 1.42)	0.61	
miRNA	AA	6 (0.74)	1 (0.12)	38.11 (3.81, 380.90)	0.002	
	AA vs (GG+GA)			38.88 (3.89, 388.23)	0.002	
	(AA+GA)	49 (6.03)	100 (12.30)	1.07 (0.68, 1.68)	0.782	
CCR7	AA	84 (10.32)	173 (21.25)	1.00 (referent)		0.458
rs3136687	GA	153 (18.80)	249 (30.59)	1.45 (0.97, 2.16)	0.07	
Intron 1	GG	42 (5.16)	113 (13.88)	0.96 (0.57, 1.62)	0.883	
	GG vs (AA+AG)			0.76 (0.49, 1.20)	0.248	
	(GG+AG)	195 (23.96)	362 (44.47)	1.30 (0.89, 1.90)	0.179	

Table 6. Validation of a Chemokine-TLR Complex Interaction along CCL5-CCR9 Axis and PCa among Men of African Descent using MDR.

Best Model (dbSNPID#)	Interactions	Cross Validation Consistency (CVC)	Average Testing Accuracy (ATA)	Permutation Testing p-value
One Factor				
CCR7_rs3136685	84	9/10	0.5827	≤0.001
Two Factor				
CCL5_rs2107538				
TLR2_rs3804099	3486	4/10	0.5892	0.044
Three Factor				
TLR4_rs1927911				
CCL5_rs3817655				
CCR9_rs41289608	95284	8/10	0.6714	≤0.001

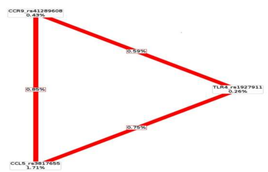

Figure 4. A Complex 3-way Chemokine-TLR Interaction was identified as the best PCa predictor among Men of African Descent. This interaction is driven a minor CCL5 and CCR9-TLR4 interaction.

SUMMARY

- Complex interactions along the IL1β-IL1α-IL1RN, IRAK4-TOLLIP, and CCL5-CCR9 axes were identified as the significant PCa predictors among cytokine, cytokine and TLR, and chemokine and TLR SNPs, respectively.
- All models revealed significant synergistic relationships using entropy based analyses.

FUTURE DIRECTIONS

- Identify new inflammatory and immune response genes that jointly modify PCa risk, disease progression, and disease recurrence among large ethnically diverse sub-groups using novel bioinformatic tools.
- Perform individual and combined inhibition of IL1β, IL1α, IRAK4, and TOLLIP expression in PCa cell lines and monitor effects on tumor behavior using preclinical models.

ACKNOWLEDGEMENTS

We thank Rick Kittles, Maria Jackson and others for contributing study participants from Washington D.C., South Carolina and Jamaica.

Grant/Research support: National Cancer Institute grant R25-CA-134283, Clinical Translational Science Pilot Grant to LRK, "Our Highest Potential" in Cancer Research Endowment to LRK, and P20-MD000175 NIH MCMHD to KSK.

Effect of Pharmacological Inhibition of Phosphoserine Aminotransferase (PSAT1) on Metastatic Breast Cancer Motility

Charles K. Castaneda[3], Susan Dougherty[1], Stephanie Metcalf[1], Brian Clem[1,2], Ph.D.,
Departments of Biochemistry & Molecular Genetics[1] and the James Graham Brown Cancer Center[2]
University of Louisville[3], Louisville, KY

UNIVERSITY OF LOUISVILLE
It's Happening Here.

ABSTRACT

Prior studies have shown that the serine biosynthesis pathway is upregulated in breast cancer cell lines, specifically, the enzyme phosphoserine aminotransferase (PSAT1). These data suggest that PSAT1 is in some way connected to breast cancer development and progression. Interestingly, additional studies have shown that silencing PSAT1 resulted in no changes in cellular proliferation; therefore, raising the question of whether PSAT1 plays some role in cellular motility and the metastasis of breast cancer cells. Based on this fact, we hypothesize that pharmacological inhibition of PSAT1 with small molecule antagonists may decrease the overall motility and metastatic character of breast cancer cells (MDA-MB-231).

To determine if PSAT1 has a functional role in cellular motility, two different assays were conducted: a wound healing assay (or scratch assay) and a motility assay. In the scratch assay, MDA-MB-231 triple-negative breast cancer cells were plated at 100K cells per well in a 24-well culture plate. The adherent monolayer of cells was subsequently "scratched" with a pipet tip and then treated with vehicle or different concentrations of PSAT1 inhibitors. The healing of the scratch was monitored, using an EVOS imaging microscope, until the scratch completely healed.

The motility assay utilized 24-well *Millipore* hanging cell inserts that contained a porous membrane. In this assay, IMEM media was placed directly into each well of a 24-well plate. Then, the inserts were placed into each well and 25k cells were plated in serum-free IMEM media directly into this insert. All inhibitors were added in equal concentrations to the serum-free and regular IMEM media solutions to prevent dilution during the assay. After 24 hours, the membrane was fixed with methanol and stained using crystal violet. Images of each membrane were then taken and compared to control inserts.

Overall, both cellular motility assays provided consistent data. However, of the eight PSAT1 inhibitors tested, none showed a significant decrease in cellular motility when compared to controls. Taken together, the results are inconclusive and neither support nor refute the proposed hypothesis that using small molecule inhibitors of PSAT1 may decrease the overall motility and metastatic nature of MDA-MB-231 breast cancer cells. Fortunately, initial testing using genetic PSAT1 suppression has shown the effects of PSAT1 inhibition in MDA-MB-231 cells. The eight inhibitors tested were only a small fraction of the molecules identified as possible antagonists of PSAT1. Therefore, looking forward, many more potential PSAT1 inhibitors await similar motility testing. Ultimately, if one of these inhibitors proves to show success in vitro, it could have future clinical relevance for the treatment of metastatic breast cancer.

INTRODUCTION

- Currently, the metastatic (stage IV) breast cancer 5-year survival rate is 26% compared to 90% and 72% for stages II and III, respectively. (www.cancer.org)
- Therefore, copious amounts of research are focused on breast cancer metastasis and understanding the underlying mechanisms which enable breast cancer cells to metastasize throughout the body.
- Of the many studies conducted, several have shown that the serine biosynthesis pathway is highly upregulated in breast cancer cell lines, specifically, the enzyme phosphoserine aminotransferase (PSAT1).
- Interestingly, additional studies have shown that silencing PSAT1 resulted in **no changes in cellular proliferation.**
- This raises the important question: Does PSAT1 play some role in **cellular motility and metastasis of breast cancer cells**.

RATIONALE

Previous studies within the lab demonstrate that PSAT1 knockdown conditions decreases overall cellular motility (MDA-MB-231 cells). The results of motility and wound healing assays **(shown in Figure 1)** illustrate this phenomenon and suggest PSAT1 has some role in motility and metastatic character. This decrease in cellular motility makes PSAT1 a good candidate for potential therapeutic targeting via pharmacological inhibition in metastatic breast cancer cells.

HYPOTHESIS

Pharmacological inhibition of PSAT1 with small molecule antagonists may decrease the overall motility and metastatic character of breast cancer cells (MDA-MB-231).

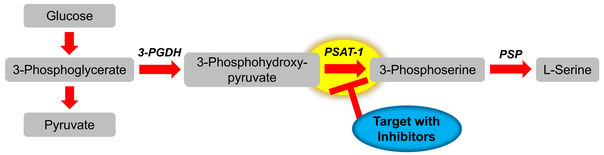

RESULTS

1

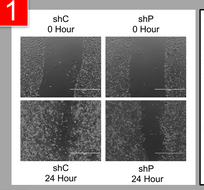

Figures 1 & 2: PSAT1 activity plays some role in the motility and metastatic character of breast cancer cells (MDA-MB-231). Both 24-hour scratch and motility assays illustrate this phenomenon in control vs. PSAT1 knockdown cells.

Data provided by Stephanie Metcalf

2

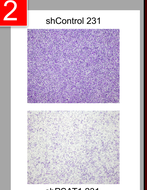

3

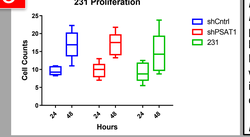

Figure 3: Proliferation Rate of PSAT1 Knockdowns. This data compares the proliferative rates between control, knockdown, and WT MDA-MB-231 cells. Because no difference was noted, PSAT1 was hypothesized to not play a major role in the proliferation rate of breast cancer cells.

Data provided by Stephanie Metcalf

4

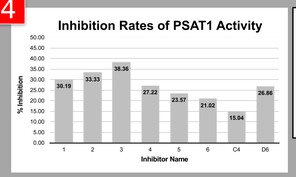

Figure 4: Relative inhibition rates of PSAT1 antagonists. Based on computational modeling, several PSAT1 inhibitors were identified. Each inhibitor was then tested in an enzymatic assay to determine relative rates of inhibition.

Data provided by Susan Dougherty

5

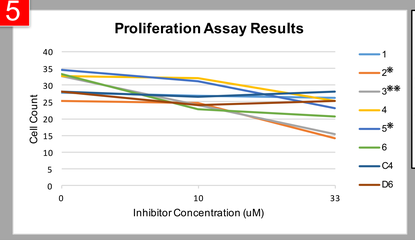

Figure 5: Proliferation Assays. A proliferation assay was conducted with each new inhibitor. The MDA-MB-231 cells were plated at 50k cells per well in a 24-well plate. After 24 hours the cells were treated with varying concentrations of each inhibitor (0.3uM, 1uM, 3uM, 10uM, 33uM, and a vehicle DMSO control). The cells were then allotted 48 hours to incubate at 37° C before being counted.
(*= p-value< 0.05)

6

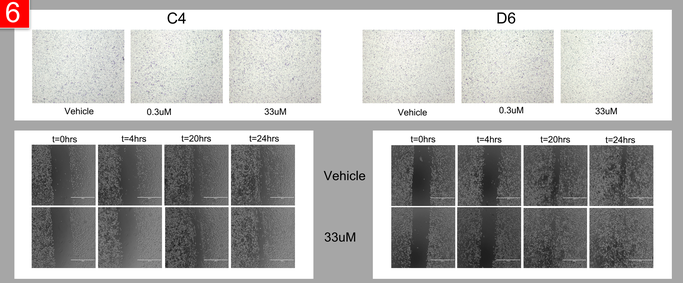

7

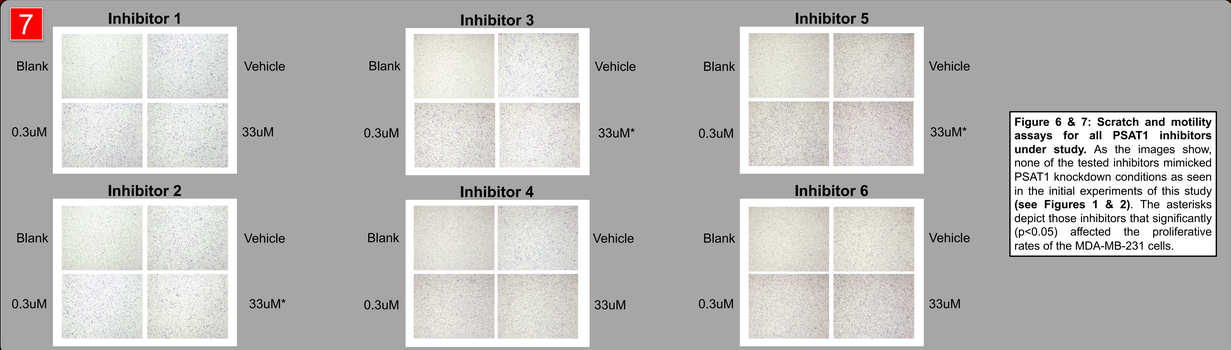

Figure 6 & 7: Scratch and motility assays for all PSAT1 inhibitors under study. As the images show, none of the tested inhibitors mimicked PSAT1 knockdown conditions as seen in the initial experiments of this study **(see Figures 1 & 2)**. The asterisks depict those inhibitors that significantly ($p<0.05$) affected the proliferative rates of the MDA-MB-231 cells.

METHODS

Scratch Assay Protocol

- MDA-MB-231 were plated at 100k cells per well into a 24-well plate.
- The cells were incubated for 24 hours at 37° C.
- Each well was scratched with a p-10 pipet tip.
- The healing of the scratch was monitored for 24 hours with an EVOS imaging microscope.

Motility Assay Protocol

Plating

- Four experimental treatment conditions (vehicle, 0.3uM, 33uM, and blank) were made using IMEM media (containing serum).
- 500uL of each treatment aliquot was then added to a 24-well plate in duplicate.
- MDA-MB-231 cells were then collected in **serum-free media**.
- Identical treatments aliquots were then made using the serum-free cell solution.
- 500uL of the serum-free solution was then added (which contained 25k cells per well and each specific treatment condition) to a 24-well *Millipore* hanging cell culture insert.
- The cells were then incubated for 24 hours at 37° C.

Harvesting

- Each insert was placed in 500uL of cold methanol 10 minutes.
- The inserts were then drained and transferred to 750uL of PBS.
- All inserts were gently washed with a PBS-wetted cotton swab (repeat 3 times).
- The inserts were drained and transferred to 500uL of crystal violet dye for 10 minutes.
- Each insert was then rinsed in PBS for 2 minutes.
- The inserts were also rinsed in MiliQ water (repeat two times).
- All inserts were then dried for 30 minutes.
- Excess liquid was aspirated off using a gel-loading pipet tip.
- The inserts then allotted an additional 24 hours to dry.
- Images of each insert were then taken using a digital inverted microscope.

DISCUSSIONS

- The results of this study are inconclusive and neither support or refute the proposed hypothesis.
- However, many more PSAT1 inhibitors await testing with the scratch and motility assay protocol used in this study.

FUTURE DIRECTIONS

- Identify more potent inhibitors of PSAT1 in order to maximize the therapeutic potential of this approach.

ACKNOWLEDGEMENTS

Research funded by the National Cancer Institute R25 CA-134283-04 Cancer Education Program Grant at the University of Louisville.

UofL Design and Print

Detection of pancreatic cancer using a modified gelatin nanocontrasting agent

Phillip Chuong, Benjamin Fouts, Molly McNally, Lacey McNally PhD.
Department of Medicine, University of Louisville

ABSTRACT

Purpose: Modern diagnostic methods of pancreatic cancer have not presented themselves as an effective option for patients due to the inherent difficulties that are associated with pancreatic cancer. These difficulties arise from the inability for most modern imaging modalities to accurately target/image the location of tumor regions and apply effective treatment. Due to these difficulties, nanotechnology has gained much interest as a possible method of tumor-targeting as well as a vehicle for drug delivery. We hypothesized that the gelatin-coated mesoporous silica nanoparticles conjugated with a targeting ligand, Syndecan-1, will provide increased detection and treatment of pancreatic cancer.

Methods: Mesoporous silica nanoparticles coated with gelatin (MSN-G) were synthesized from a colloidal mixture of cetyl trimethylammonium bromide (CTAB) along with tetraethyl orthosilicate (TEOS). Desired pores were formed through a series of dialysis processes. A gelatin coat was synthesized and formed encircling the MSN. The MSN-G were modified to contain a fluorescent dye and incorporate a targeting-ligand protein for the IGF1 receptor. Several methods were utilized to characterize the MSN-G including Energy-dispersive x-ray spectroscopy (EDX), UV-Vis Spectroscopy, and Transmission Electron Microscopy (TEM). Pancreatic cancer cell-lines, S2VP10L and Panc1, were given varied concentrations of Matrix Metalloproteinase-2 (MMP2) and Protease Inhibitor and then treated with the conjugated MSN-G. Odyssey infrared imaging was utilized to determine the binding ability of the Syndecan-1 ligand and the degradation interaction between the MMP2 and gelatin coat. Furthermore, S2VP10L cells, containing the IR-780 dye encapsulated by the MSN-G were transferred into tissue phantoms and imaged using Multispectral Optoacoustic Tomography (MSOT).

Results: TEM images along with Dynamic Light Scattering (DLS) results demonstrated that the MSN-G were approximately 35 nm in size as detected by the two techniques, indicating the successful encapsulation of the MSN with the gelatin coat. Odyssey infrared imaging displayed increased signaling at higher concentrations of MMP2. This increased signaling demonstrated the higher level of gelatin degradation from the MMP2 enzymatic activity compared to lesser amount of degradation found in the presence of the Protease Inhibitor. Signaling at MMP2 displayed approximately 48 times and 16 times greater binding intensity compared to the MMP Inhibitor trial for S2VP10L and Panc1 respectively. MSN-G were placed into tissue phantoms and imaged via MSOT. A spectrum for the MSN-G encapsulated with IR-780 dye was obtained.

Conclusion: IGF1 receptor targeted, gelatin-coated MSNs were found to possess substantial tumor cell binding against multiple cell lines and demonstrate potential as a theranostic nanocontrasting agent for pancreatic cancer.

Synthesis of Syndecan-1 Conjugated MSN-G Schematic

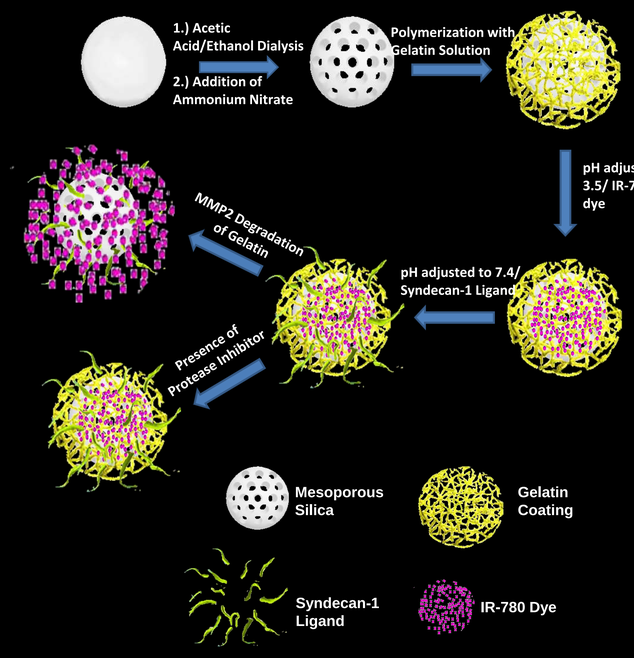

Elevated levels of MMP2 results in gelatin degradation and release of IR-780 dye. Inhibition of MMP2 enzymatic activity results in less significant release of dye.

RESULTS

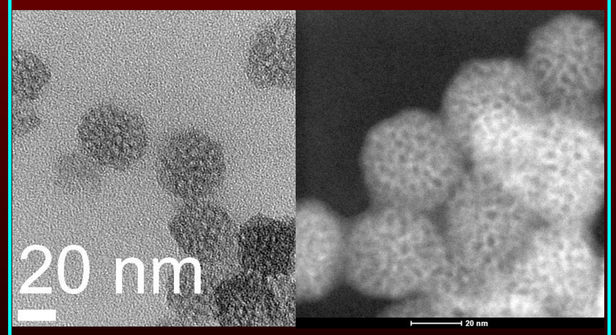

Figure 1: Transmission electron microscopy (TEM) and Scanning transmission Electron Microscopy (STEM) imaging of gelatin-coated MSNs (MSN-G). MSN particles contained visible mesoporous, spherical structures with a diameter of ~35 nm and a pore size of ~2 nm. Gelatin-coating was confirmed in the increase in size of the particle.

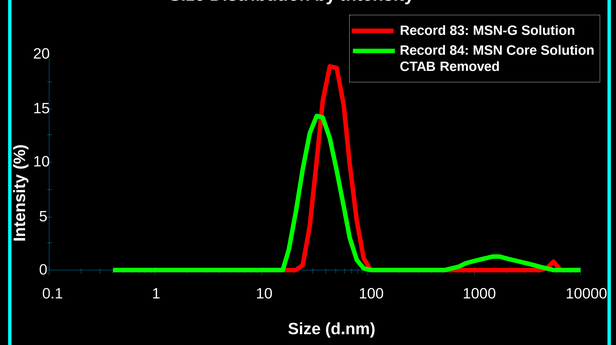

Figure 2: Dynamic Light Scattering (DLS) results demonstrated the MSNs to have a size of ~38 nm. After encapsulation with a gelatin coat, the newly synthesized MSN-G displayed a size of ~ 49 nm. The notable increase in size aided in the conformation of successful encapsulation of the gelatin-coat on the MSN.

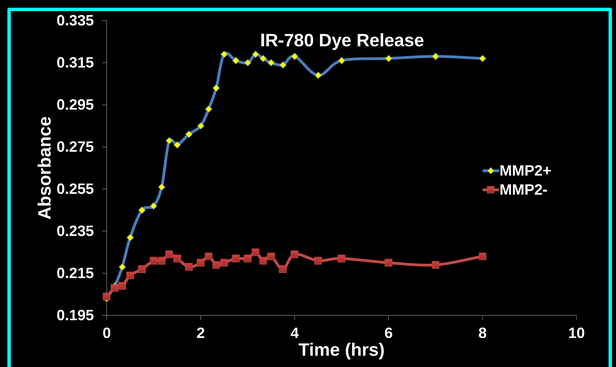

Figure 3: Evaluation of gelatin degradation and IR-780 dye release from MSN-G. A 2mL sample of Syndecan-1 conjugated MSN-G were placed into dialysis tubing and dialyzed in a solution of PBS 7.4. A 10 µg/12 µL solution of MMP2 was introduced into the particle solution and absorbance was measured by UV-Vis Spectroscopy over a period of 8 hrs. Optimal absorbance intensity of the IR-780 dye was found at ~2.5 hours. The MSN-G exhibited ~1.5 times greater dye release in the MMP2+ trial compared to MMP2-. This selective release illustrates the selective gelatin degradation found between MMP2 and the MSN-G.

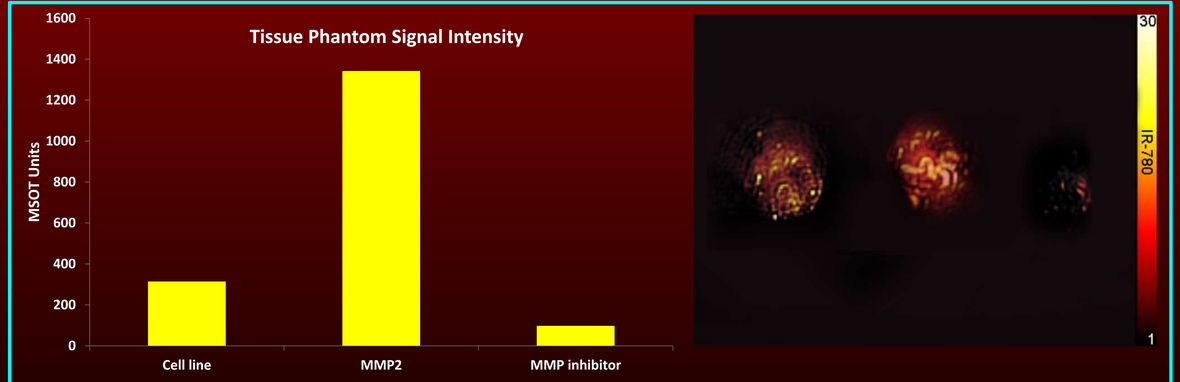

Figure 7: Visualization of targeted MSN binding to IGF1 positive cells using phantoms with MSOT and cells incubated with 50 µL of MSN-G for 1 hour. Cells were washed and inserted into tissue phantoms and signal intensity was determined using MSOT. The resulting graphs display greater signal intensity present in the MMP2 well compared to the cells alone and MMP Inhibitor.

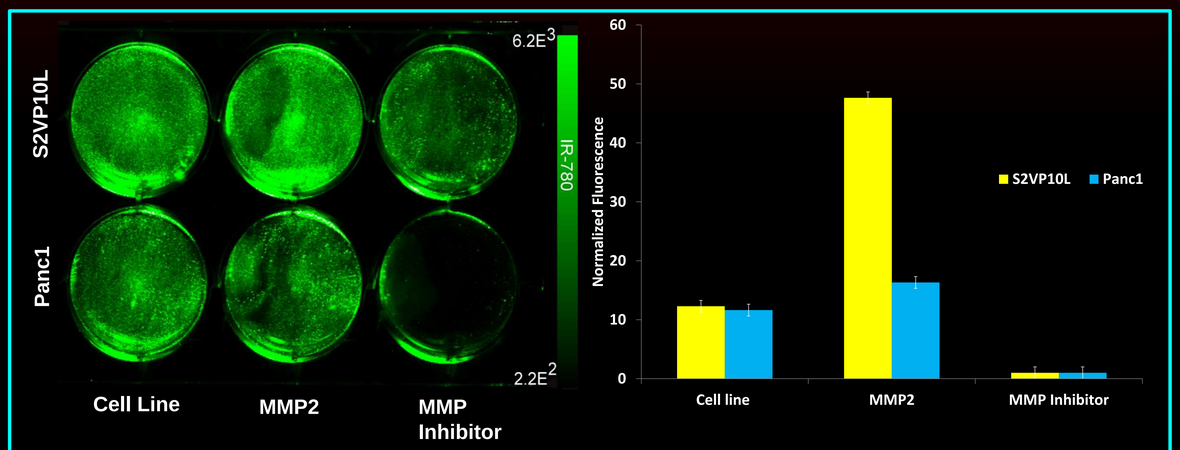

Figure 6: Odyssey infrared imaging displayed significant difference in the level of signal intensity between varied concentrations of MMP2 for IR-780 dye conjugated MSN-G. Approximately 48 times greater for S2VP10L and 16 times greater for Panc1

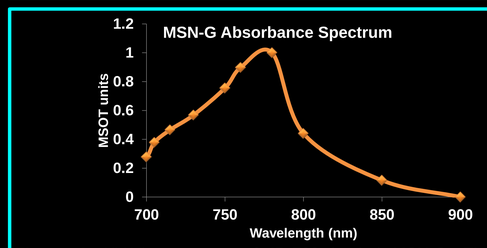

Figure 4: UV-Vis spectrum of IR-780 loaded MSN-G. The graph demonstrates an absorbance peak of ~780 nm. The identification of the 780 nm peak indicates the successful loading of IR-780 dye into the MSN-G and confirms the fluorescent capabilities of this particle.

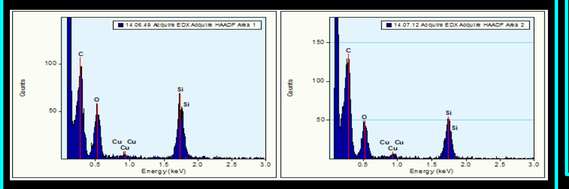

Figure 5: Energy-dispersive x-ray spectroscopy (EDX) of the MSN-G confirmed the presence of biocompatible and more importantly non-cytotoxic elements found in the MSN-G. The structure of the MSN-G consist of mainly silica, carbon, and oxygen.

CONCLUSION

- Theranostic nanoparticles provide the benefits of enhanced tumor detection along with serving as a vehicle to transport chemotherapeutics
- A biological marker found in aggressive cancer lines is the elevated levels of Matrix Metalloproteinase 2, a gelatinase, and their corresponding enzymatic activity of degrading gelatin compounds
- This study demonstrated the successful synthesis of gelatin-coated mesoporous silica nanoparticles (MSN-G) conjugated with a Syndecan-1 ligand for theranostic imaging of pancreatic cancer
- The MSN-G displayed selectively enhanced gelatin degradation in the presence of MMP2 for multiple cell lines in *in vitro* studies for both odyssey infrared imaging and tissue phantoms
- Further studies involve in-depth characterizations studies of the MSN-G and continuation into *in vivo* studies

ACKNOWLEDGEMENTS

This work was supported by NCI Grant CA139050 and NIH/NCI GRANT R25 - CA134283